Journal of Mechanical and Energy Systems (JMES)
ISSN 3163-3846
Volume 3 Nomor 01, 2026

ANALYSIS OF GRAPHITE: PVA-BASED TRANSPARENT ELECTRODES WITH DMSO ADDITIVE FOR TRANSPARENT SOLAR-CELL APPLICATIONS

Navy Anan Diano[1]*, Aris Ansori[1], Indra Herlamba Siregar[1],
Aris Purwanto[1], Edy Herianto[2]
[1]Mechanical Engineering Study Program, Faculty of Engineering, Universitas Negeri Surabaya, Ketintang, Surabaya 60231, Indonesia
[2] Fuel Cell Institute, The National University of Malaysia, Bandar Baru Bangi, Hulu Langat District, Selangor, Malaysia.

***Corresponding author**
navy.22114@mhs.unesa.ac.id

Graphical Abstract

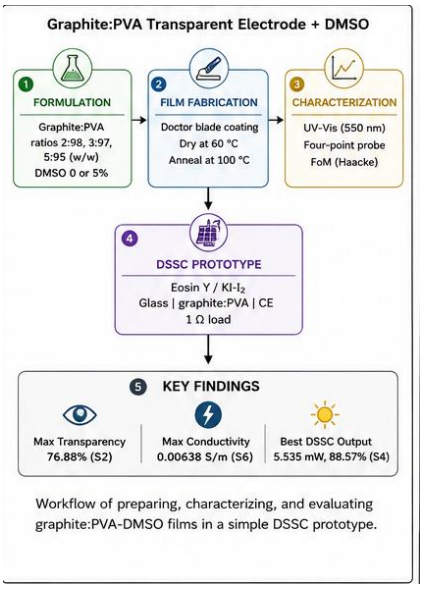

Abstract

Transparent electrodes must combine optical transmission and electrical conduction, but low-cost carbon-polymer films commonly exhibit a trade-off between these properties. This study evaluates graphite:polyvinyl alcohol (PVA) composite films containing dimethyl sulfoxide (DMSO) and examines their preliminary applicability in a simple dye-sensitized solar-cell (DSSC) prototype. Six films were prepared on glass using nominal graphite:PVA ratios of 2:98, 3:97, and 5:95, each with 0 or 5% DMSO. The films were deposited by doctor blade and annealed at 100 °C. Optical transparency was determined from UV-Vis absorbance at 550 nm, electrical conductivity was measured by four-point probe, and the optoelectronic balance was assessed using the Haacke figure of merit (FoM). The films were then incorporated into Eosin-Y/KI-I2 prototype cells and tested under a halogen lamp with a 1 Ω load. DMSO increased conductivity at every graphite ratio, while its effect on transparency depended on graphite loading. S2 (2:98, 5% DMSO) provided the highest transparency (76.88%) and FoM (2.02×10^{-9}), whereas S6 (5:95, 5% DMSO) provided the highest conductivity (0.00638 S/m). Device-level performance did not follow FoM directly: S4 (3:97, 5% DMSO) yielded the highest reported output power (5.535 mW) and simple output-to-input ratio (88.57%). The results support graphite:PVA-DMSO as an exploratory low-cost electrode platform, while emphasizing that thickness control, morphology characterization, calibrated illumination, and replicated I-V testing are required for photovoltaic validation.

Keywords: transparent electrode; graphite-PVA composite; DMSO; optical transparency; DSSC

Article history: Received: 7 July 2026, Received in revised: 15 August 2025, Accepted: 16 August 2026, Published online: 17 August 2026

1. Introduction

Transparent electrodes are essential components in optoelectronic and energy-conversion systems because they must transmit incident light while providing a continuous path for electrical charge. Conventional transparent conducting oxides, particularly indium tin oxide (ITO), remain widely used because of their high optical transmission and low sheet resistance. However, the limited availability and cost of indium, the brittleness of oxide layers, and the processing demands of vacuum-based deposition motivate the search for alternative transparent-electrode systems [1]-[4]. Carbon-based fillers dispersed in polymer matrices are attractive for exploratory low-cost electrodes because they can be processed from solution, deposited over comparatively large areas, and tuned through composition and solvent engineering [5]-[8].

Carbon-polymer composites are governed by a competition between optical transmission and electrical connectivity. As the conductive-filler fraction increases, particle-to-particle contacts become more probable and a percolated electrical network can form; at the same time, absorption and scattering by the carbon phase can reduce visible-light transmission [7], [8], [17]. Choi et al. [8] demonstrated that the percolation threshold of carbon black depends strongly on the polymer matrix, reporting thresholds of approximately 0.58 wt% in PET, 0.97 wt% in PP, and 3.17 wt% in nylon. This matrix dependence is important because it

shows that conductive-network formation cannot be inferred from filler content alone; dispersion, interfacial compatibility, and processing history also influence the transition from isolated particles to a continuous conducting pathway [7], [17].

Previous carbon/PVA studies reinforce the importance of filler dispersion and polymer-filler interactions. Alhuthali et al. [5] examined PVA/graphene nanocomposites, while Zor et al. [6] reported PVA films containing carbonized waste-rubber filler. Conductive PVA nanocomposites containing multiwalled carbon nanotubes have also been prepared and characterized, demonstrating that a water-processable PVA matrix can host conductive carbon networks when the filler is sufficiently interconnected [16]. These studies collectively indicate that the electrical response of PVA-based carbon composites depends not only on the intrinsic conductivity of the carbon phase but also on how effectively conductive pathways are established within the polymer matrix.

Carbon materials have also been explored directly in electrochemical and photovoltaic electrodes. Carbon-based composite electrodes have been investigated for electroanalytical applications because of their chemical stability, conductive character, and processability [15]. In DSSC research, carbonaceous counter-electrode systems, including graphite-, soot-, graphene-, and reduced-graphene-oxide-based structures, have been investigated as lower-cost alternatives to conventional noble-metal electrodes [18]. The thesis underlying the present work also identifies previous DSSC studies in which candle-soot carbon produced a relatively homogeneous counter-electrode morphology and in which graphite-containing PVA systems improved ionic transport. These findings support the broader premise that carbon materials can contribute to charge-transfer pathways in solution-processed solar-cell components, although the role of carbon depends on whether it functions as a transparent current collector, counter electrode, or electrolyte additive.

Polyvinyl alcohol (PVA) is attractive as a matrix because it is water-processable, has strong film-forming ability, adheres to glass, and contains hydroxyl groups capable of interacting with carbon surfaces. In a graphite:PVA film, PVA mechanically binds the dispersed graphite while graphite provides the principal conductive phase. Dimethyl sulfoxide (DMSO), a polar aprotic solvent, can modify polymer-chain organization and particle wetting. In conductive-polymer/PVA blends, DMSO has been associated with improved charge transport and more effective conductive pathways [9]. Nevertheless, the magnitude and even the optical direction of the DMSO effect can vary with solids loading and coating morphology, so its influence must be evaluated at each graphite composition rather than assumed to be universal.

Dye-sensitized solar cells (DSSCs) provide a practical platform for testing whether a film that appears promising at the material level can function in an assembled light-to-electricity device. A DSSC combines a sensitizing dye, an electron-transporting photoelectrode, a redox electrolyte, and a counter electrode [10], [11]. Device output is therefore influenced not only by the transparent film but also by dye coverage, electrolyte distribution, interfacial contact, internal resistance, illumination uniformity, and assembly quality. Accordingly, a film with the best material-level figure of merit does not necessarily produce the best prototype output.

The novelty of this study is the integrated assessment of solution-processed graphite:PVA films with DMSO at both the film and prototype-device levels using a simple doctor-blade route on ordinary glass. Six compositions were compared for UV-Vis optical response, electrical conductivity, and Haacke figure of merit, and were subsequently incorporated into simple Eosin-Y-sensitized DSSC prototypes. The main objective was to determine how graphite ratio and DMSO addition influence the optoelectronic balance of the film and to identify the formulation that produces the best reported response after device integration.

2. Material and Method

2.1. Materials and Experimental Design

The study used graphite powder as the conductive filler, PVA as the film-forming matrix, distilled water as the main solvent, DMSO as an additive, and ordinary glass as the substrate. The device-application stage used Eosin Y as the sensitizer, potassium iodide (KI) and iodine (I2) in ethylene glycol as the redox electrolyte, and candle soot deposited on a second glass plate as the counter electrode. The principal instruments were a magnetic hotplate, an oven, a UV-Vis spectrophotometer, a four-point-probe system, a lux meter, and a digital multimeter.

A two-factor formulation matrix was employed. The nominal graphite:PVA ratios were 2:98, 3:97, and 5:95, and each ratio was prepared without DMSO or with 5% DMSO. The six combinations were coded S1-

S6. The independent variables were graphite ratio and DMSO concentration, while the measured responses were absorbance/transparency, conductivity, figure of merit, light-input power, electrical-output power, and the simple output-to-input ratio of the assembled prototype.

Table 1. Formulation codes for graphite:PVA-DMSO films

Sample	Graphite:PVA	DMSO (%)	Description
S1	2:98	0	Low graphite, without DMSO
S2	2:98	5	Low graphite, with DMSO
S3	3:97	0	Intermediate graphite, without DMSO
S4	3:97	5	Intermediate graphite, with DMSO
S5	5:95	0	High graphite, without DMSO
S6	5:95	5	High graphite, with DMSO

2.2. Control of Experimental Variables

To strengthen comparability among formulations, the principal process and testing variables were defined as controlled conditions. All coatings used the same doctor-blade procedure on ordinary glass: adhesive tape was positioned along the substrate edges to define the coating gap, the dispersion was deposited on the glass, and the blade was drawn in one direction. The same substrate type and nominal annealing temperature of 100 °C were used for all samples. UV-Vis measurements were carried out with the same instrument and measurement range, while four-point-probe measurements used the same instrument configuration, measurement approach, and sampling procedure.

For the DSSC stage, the active area (0.000625 m^2), nominal lamp arrangement, measurement instruments, and 1 Ω load were kept the same. The illumination source was a 1000 W halogen lamp positioned nominally at the same geometry for each test. However, the measured incident-light input was not identical among samples (5.375-6.294 mW). Therefore, illumination is described here as a nominally controlled variable rather than perfectly constant, and the device results are interpreted as exploratory within this experimental setup. This distinction is important because uncontrolled variation in incident light can alter the calculated output-to-input ratio.

2.3. Film Preparation

A 5% PVA stock solution was prepared by adding 0.50 g of PVA gradually to 10 mL of distilled water heated to approximately 100 °C. The mixture was stirred for 60 min at approximately 560 rpm until visually homogeneous and was then cooled to room temperature. Graphite was weighed according to the target composition and introduced into the PVA solution while the stirring rate was increased to approximately 700 rpm. For DMSO-containing formulations, DMSO was subsequently added and mixing was continued for approximately 50 min. Each mixture was stirred for a further 20 min and then allowed to stand for about 5 min to reduce entrained bubbles.

Glass substrates were cleaned using alcohol and distilled water and were dried before coating. Adhesive tape was placed along both sides of each substrate to define the coating gap. The graphite:PVA dispersion was dropped onto the glass and drawn in one direction using a glass blade. The tape was removed carefully, and the coated substrates were dried and annealed in an oven at 100 °C for 30-60 min. The overall workflow is shown in Figure 1.

Figure 1. Original graphite:PVA-DMSO film samples S1-S6.

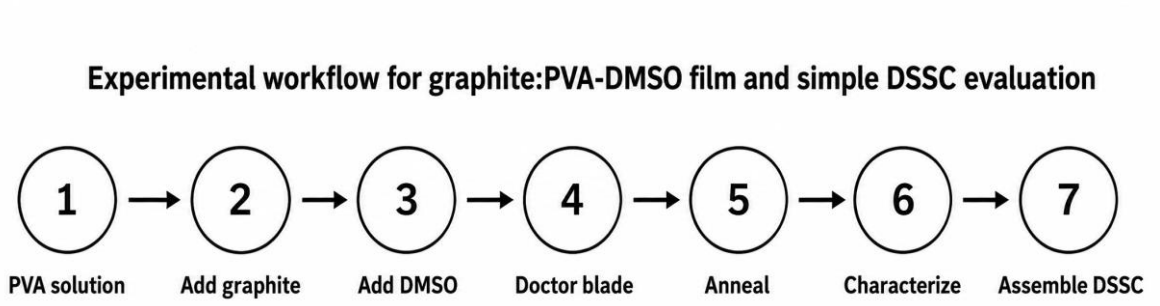

Figure 2. Experimental workflow for film preparation, characterization, and prototype evaluation.

2.4. Optical and Electrical Characterization

Optical measurements were conducted using a UV-Vis spectrophotometer over the 325-800 nm range reported in the thesis. The instrument output was absorbance. For direct comparison among formulations, absorbance at 550 nm was selected as a representative visible-light value and converted to percentage transmittance using T(%) = 10^(-A) × 100, where A is absorbance. The complete wavelength range was used during measurement, but the present quantitative inter-sample comparison is based on the 550 nm point.

$$\mathrm{T}\ (\%) = 10\text{^}(\text{-A}) \times 100\% \quad (1)$$

where A is absorbance and T is optical transmittance.

Electrical conductivity was measured using a four-point-probe method. The mean conductivity reported for each sample was used for comparison. The optoelectronic balance was assessed using the Haacke figure of merit, FoM = T^10/Rs, where T is transmittance in decimal form and Rs is sheet resistance. Because transmittance is raised to the tenth power, this metric strongly penalizes films with low optical transmission.

$$\mathrm{FoM} = \mathrm{T}\text{^}10 \ / \ \mathrm{R_s} \quad (2)$$

where T is transmittance in decimal form and R□ is sheet resistance (Ω/sq).

2.5. Simple DSSC Prototype Assembly and Testing

The coated electrode was sensitized by applying Eosin Y to the active region and drying it at room temperature for approximately 60 min. A counter electrode was prepared by exposing a cleaned glass plate to a candle flame until a soot layer formed while leaving an uncovered edge for electrical contact. The electrolyte was prepared by dissolving 0.8300 g KI in approximately 7 mL ethylene glycol at 40 °C and 350

rpm for 15 min, adding 0.1269 g I2, stirring for another 15 min, and adjusting the final volume to 10.0 mL with ethylene glycol.

The sensitized electrode and soot-coated counter electrode were assembled face-to-face in a slightly offset sandwich configuration and secured with binder clips. One to two drops of KI/I2 electrolyte were introduced from the side. Open-circuit voltage and loaded voltage were measured with a digital multimeter, and a 1 Ω resistor was used for the loaded condition. Output power was calculated as Pout = Vload × I, while input power was obtained from the irradiance value used in the thesis multiplied by the active area. The reported simple ratio, ηsimple = (Pout/Pin) × 100%, is used only for within-experiment comparison because illumination was not calibrated to a standard photovoltaic spectrum and no complete current-voltage sweep was performed.

$$\eta\_simple = (P\_out / P\_in) \times 100\% \quad (3)$$

$$P\_out = V\_load \times I \quad (4)$$

$$P\_in = I\_irradiance \times A\_active \quad (5)$$

3. Result and Discussion

3.1. UV-Vis Spectroscopy and Optical Transparency

UV-Vis spectroscopy provided the direct spectroscopic evidence available in this study. Measurements were collected over 325-800 nm, and the absorbance at 550 nm was used for quantitative comparison. The measured absorbance values were 0.33791 (S1), 0.11418 (S2), 0.14537 (S3), 0.38915 (S4), 0.36740 (S5), and 0.44213 (S6), corresponding to calculated transmittances of 45.93%, 76.88%, 71.55%, 40.82%, 42.91%, and 36.13%, respectively. Thus, S2 showed the lowest absorbance and highest transparency, whereas S6 showed the highest absorbance and lowest transparency.

The overall trend is consistent with the optical penalty expected when the concentration or connectivity of carbon particles increases. More graphite can increase absorption and scattering, thereby lowering the fraction of visible light transmitted through the coating. Nevertheless, graphite content was not the only governing factor. At 2:98, adding DMSO increased transparency from 45.93% (S1) to 76.88% (S2), whereas at 3:97 and 5:95 the addition of DMSO reduced transparency. This composition-dependent response suggests that DMSO altered particle wetting and film formation differently at different solids loadings.

S3 is noteworthy because it retained high transparency despite a higher nominal graphite content than S1 and S2. The result indicates that coating thickness and local uniformity may also contribute to the optical response. Because dry-film thickness was not measured by profilometry, the present data cannot separate composition effects from thickness effects. Future work should report controlled dry-film thickness together with full wavelength-dependent transmittance spectra.

Table 2. Spectroscopic, optical, and electrical characteristics of graphite:PVA-DMSO films

Sample	Absorbance 550 nm	Transparency (%)	Conductivity (S/m)	Sheet resistance (Ω/sq)	FoM
S1	0.33791	45.93	0.000267988	289,233,260.5	1.41×10^{-12}
S2	0.11418	76.88	0.003792767	35,653,006.36	2.02×10^{-9}
S3	0.14537	71.55	0.001866419	35,106,764.19	1.00×10^{-9}
S4	0.38915	40.82	0.003443690	34,004,934.57	3.78×10^{-12}
S5	0.36740	42.91	0.002140647	32,385,064.87	6.53×10^{-12}
S6	0.44213	36.13	0.006378564	35,247,927.20	1.08×10^{-12}

3.2. Electrical Conductivity and Figure of Merit

The reported mean electrical conductivity ranged from 0.000267988 S/m for S1 to 0.006378564 S/m for S6. In films without DMSO, conductivity increased with graphite loading: 0.000268 S/m for S1, 0.001866 S/m for S3, and 0.002141 S/m for S5. This tendency is consistent with the progressive establishment of conductive contacts and the general percolation behavior reported for carbon-filled polymer systems [7], [8], [17].

DMSO increased conductivity at every matched graphite ratio. At 2:98, conductivity increased from 0.000268 S/m in S1 to 0.003793 S/m in S2; at 3:97, from 0.001866 S/m in S3 to 0.003444 S/m in S4; and at 5:95, from 0.002141 S/m in S5 to 0.006379 S/m in S6. This consistent electrical improvement is compatible with literature describing solvent-assisted improvements in charge transport in DMSO-modified conductive-polymer/PVA films [9]. However, without direct morphology measurements, the specific mechanisms—

improved graphite dispersion, polymer-chain rearrangement, reduced interparticle spacing, or some combination—cannot be distinguished experimentally in the present work.

The transparency-conductivity relationship was non-linear. S6 combined the highest conductivity with the lowest transparency, illustrating the expected trade-off. S2 was distinctive because it combined high transparency with relatively high conductivity, while S3 combined high transparency with moderate conductivity. The Haacke FoM therefore ranked S2 highest at 2.02×10^{-9}, followed by S3 at 1.00×10^{-9}; the other samples were in the 10^{-12} range. These values are best interpreted as a relative ranking within the present experiment rather than as performance equivalent to commercial transparent conductors.

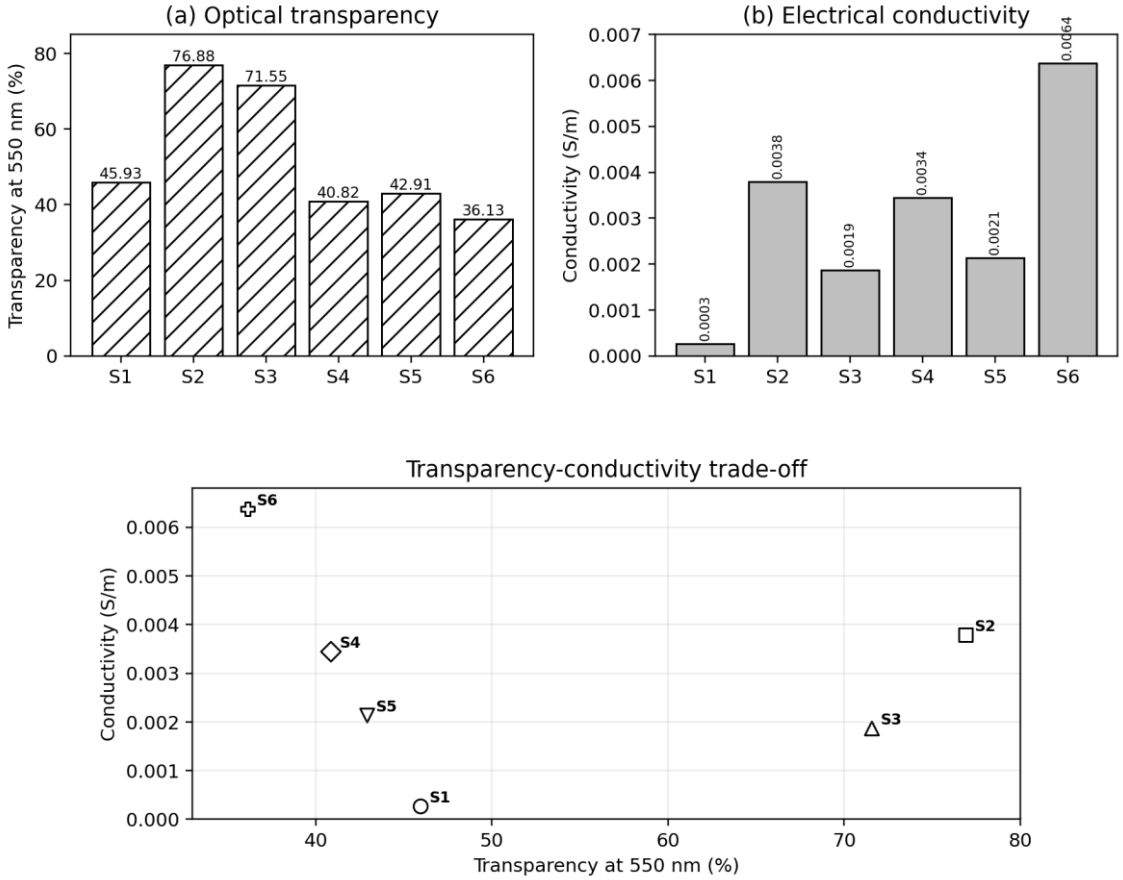

Figures 3-4. Optical transparency, electrical conductivity, and transparency-conductivity trade-off of the six films.

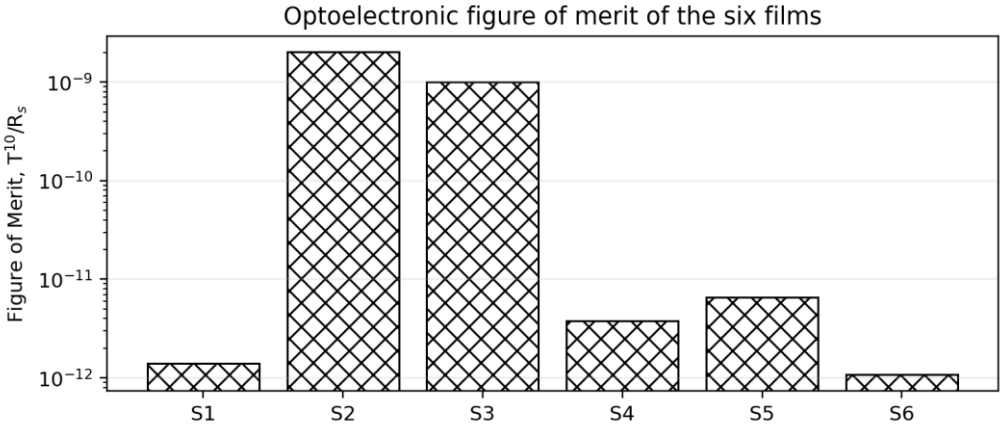

Figure 5. Haacke optoelectronic figure of merit of the six films.

3.3. Microstructural Evidence and Characterization Limitation

No SEM, AFM, profilometry, FTIR, Raman, or XRD characterization was performed in the underlying thesis. Consequently, the present study does not provide direct microstructural images, measured surface roughness, dry-film thickness, or chemical/structural spectra beyond UV-Vis. Statements concerning graphite

agglomeration, particle dispersion, film morphology, and conductive-network formation are therefore interpretations inferred from the combined optical and electrical trends and from established carbon-polymer literature [7], [8], [16], [17], not direct microstructural observations.

This limitation is particularly relevant to S2, S3, and S6. The unusual combination of high transparency and useful conductivity in S2, the high transparency of S3 despite higher graphite content, and the strong conductivity but low transparency of S6 can plausibly be influenced by differences in coating thickness, particle distribution, and local network connectivity. Direct SEM or AFM imaging, thickness profilometry, and complementary FTIR or Raman analysis would be required to verify these mechanisms. Thus, UV-Vis spectroscopy in this work establishes the optical response, while the proposed microstructural explanation should be treated as a testable hypothesis for follow-up characterization rather than as confirmed evidence.

3.4. Prototype DSSC Performance

The calculated incident-light input varied from 5.375 to 6.294 mW across the six measurements, confirming that illumination was not perfectly uniform despite the nominally fixed lamp arrangement. The reported output power ranged from 3.014 to 5.535 mW. S4 yielded the highest output power (5.53536 mW), narrowly exceeding S3 (5.49081 mW). S2 produced 4.52929 mW, while S1, S5, and S6 produced 3.844, 3.50464, and 3.01401 mW, respectively. The corresponding simple output-to-input ratios were 88.57% for S4, 88.21% for S3, 84.27% for S2, 62.76% for S1, 55.68% for S5, and 51.85% for S6.

The device ranking did not match the material-level FoM ranking. S2 had the highest FoM but lower output power than S3 and S4, whereas S4 had a relatively low FoM because of its lower transparency yet gave the highest prototype output. This difference shows that the assembled device was affected by factors beyond bulk film transparency and conductivity, including effective contact area, continuity of the electrode at the clip connection, dye coverage, soot-counter-electrode quality, electrolyte penetration, sealing, and internal resistance.

The simple ratios reported here are not certified photovoltaic power-conversion efficiencies. Light input was estimated from the irradiance treatment used in the thesis rather than from an AM1.5G-calibrated solar simulator, and electrical output was not obtained from a complete I-V curve. Therefore, these data are appropriate for relative screening within this experiment but should not be directly compared with standardized DSSC efficiencies. A validated efficiency claim would require calibrated irradiance, a masked active area, repeated I-V sweeps, and reporting of Voc, Jsc, fill factor, series resistance, and shunt resistance [10], [11].

Table 3. Reported simple DSSC prototype performance under the study conditions

Sample	Pin (mW)	Pout (mW)	ηsimple (%)	Rank
S1	6.125	3.844	62.76	4
S2	5.375	4.52929	84.27	3
S3	6.225	5.49081	88.21	2
S4	6.250	5.53536	88.57	1
S5	6.29375	3.50464	55.68	5
S6	5.8125	3.01401	51.85	6

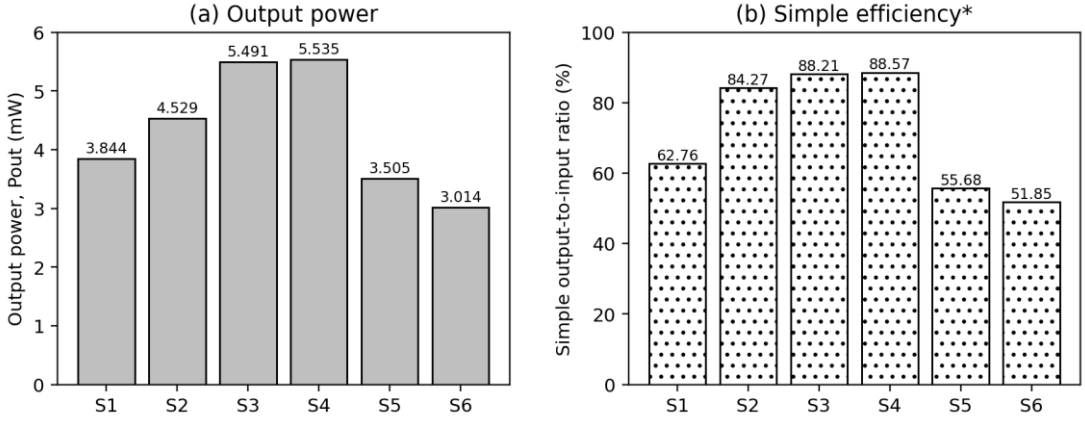

Figure 6. Reported prototype output power and simple output-to-input ratio under non-standard illumination.

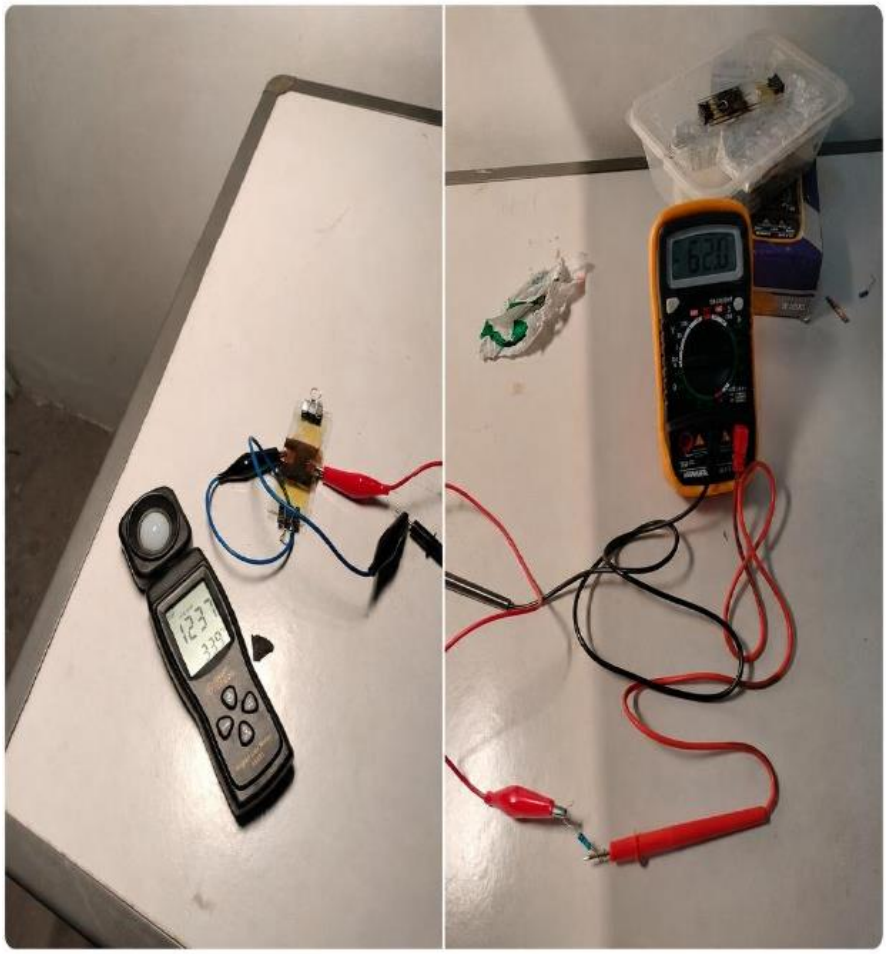

Figure 7. Original experimental setup for testing the simple DSSC prototype.

3.5. Integrated Selection of the Optimum Sample

The optimum sample depended on the evaluation level. For the film alone, S2 was preferred because it had the highest transparency and FoM while maintaining useful conductivity. For the assembled prototype, S4 was preferred because it produced the highest reported output power and simple ratio. This distinction is important: FoM is a film-level quality indicator, whereas prototype output is a system-level response. Selecting a transparent electrode for a device therefore requires both intrinsic film characterization and integration testing.

Based on the reported data, S4 (graphite:PVA 3:97 with 5% DMSO) was selected as the overall experimental optimum for the simple DSSC application. Its composition may have provided a useful compromise between a conductive carbon network and optical loss; however, this mechanism has not been directly verified morphologically. The difference between S4 and S3 was also small, and the lack of replicated device statistics prevents a definitive superiority claim. Future experiments should use independently fabricated replicates, randomized testing order, stricter illumination control, measured dry-film thickness, and statistical analysis capable of separating graphite, DMSO, and interaction effects.

4. Conclusion

Graphite:PVA-DMSO films demonstrate that a low-cost, water-processable carbon-polymer formulation can be tuned to shift the balance between optical transmission and electrical conduction. S2 (2:98 with 5% DMSO) gave the strongest film-level optoelectronic balance, with 76.88% transparency at 550 nm and the highest Haacke FoM of 2.02×10^{-9}, whereas S6 (5:95 with 5% DMSO) produced the highest conductivity of 0.006378564 S/m but the lowest transparency. At the prototype level, S4 (3:97 with 5% DMSO) produced the highest reported output power of 5.53536 mW and simple output-to-input ratio of 88.57%.

The broader take-away is that optimizing a transparent electrode cannot rely on conductivity, transparency, or FoM alone once the film is integrated into a device. The divergence between S2 at the film level and S4 at the prototype level indicates that interfacial contact, coating uniformity, electrolyte distribution, and assembly quality can become equally important. Practically, graphite:PVA-DMSO offers an

accessible solution-processed platform for exploratory transparent-electrode and educational/simple DSSC development, but the present results should not yet be interpreted as a replacement for commercial ITO/FTO or as validated photovoltaic efficiency. Progress toward that goal requires controlled and measured film thickness, direct morphology characterization, complementary spectroscopy, calibrated illumination, improved sealing/contact design, replicated devices, and complete I-V characterization.

Acknowledgment

The authors acknowledge the Mechanical Engineering Study Program, Faculty of Engineering, Universitas Negeri Surabaya, and the laboratory personnel who supported the film-characterization and prototype-testing activities.

References

[1] M. Althumayri, R. Das, R. Banavath, L. Beker, A. M. Achim, and H. C. Koydemir, "Recent advances in transparent electrodes and their multimodal sensing applications," Advanced Science, 2024, doi: 10.1002/advs.202405099.

[2] J. Wan et al., "Solution-processed transparent conducting electrodes for flexible organic solar cells with 16.61% efficiency," Nano-Micro Letters, vol. 13, no. 1, 2021, doi: 10.1007/s40820-020-00566-3.

[3] K. Sakamoto, H. Kuwae, N. Kobayashi, A. Nobori, S. Shoji, and J. Mizuno, "Highly flexible transparent electrodes based on mesh-patterned rigid indium tin oxide," Scientific Reports, vol. 8, no. 1, 2018, doi: 10.1038/s41598-018-20978-x.

[4] J. Sun and J. J. Jasieniak, "Semi-transparent solar cells," Journal of Physics D: Applied Physics, vol. 50, no. 9, 2017, doi: 10.1088/1361-6463/aa53d.

[5] A. M. S. Alhuthali, H. Kalil, and M. A. Ibrahim, "Evaluating the reactivity of polyvinyl alcohol/graphene nanocomposites," Optical Materials, vol. 151, 2024, doi: 10.1016/j.optmat.2024.115364.

[6] M. Zor, F. Şen, Z. Candan, E. Ivanov, T. Batakliev, V. Georgiev, and D. Menseidov, "Preparation and characterization of polyvinyl alcohol (PVA)/carbonized waste rubber biocomposite films," Polymers, vol. 16, no. 8, 2024, doi: 10.3390/polym16081050.

[7] Z. Zhang, L. Hu, R. Wang, S. Zhang, L. Fu, M. Li, and Q. Xiao, "Advances in Monte Carlo method for simulating the electrical percolation behavior of conductive polymer composites with a carbon-based filling," Polymers, vol. 16, no. 4, 2024, doi: 10.3390/polym16040545.

[8] H. J. Choi, M. S. Kim, D. Ahn, S. Y. Yeo, and S. Lee, "Electrical percolation threshold of carbon black in a polymer matrix and its application to antistatic fibre," Scientific Reports, vol. 9, no. 1, 2019, doi: 10.1038/s41598-019-42495-1.

[9] S. Sau and S. Kundu, "Fabrication of highly stretchable salt and solvent blended PEDOT:PSS/PVA free-standing films: non-linear to linear electrical conduction response," RSC Advances, vol. 14, no. 8, pp. 5193-5206, 2024, doi: 10.1039/D3RA08260A.

[10] W. Vallejo, M. Lerma, and C. Díaz-Uribe, "Dye sensitized solar cells: Meta-analysis of effect sensitizer-type on photovoltaic efficiency," Heliyon, vol. 11, no. 1, 2025, doi: 10.1016/j.heliyon.2024.e41092.

[11] D. M. Atia and N. M. Ahmed, "Mathematical modeling, parameter identification, and electrical performance of a DSSC based on nature-inspired optimization techniques," Journal of Computational Electronics, vol. 22, no. 2, pp. 723-741, 2023, doi: 10.1007/s10825-023-02018-8.

[12] S. Boscarino et al., "Cu metal nanoparticles in transparent electrodes for light harvesting in solar cells," Applied Surface Science, vol. 655, 2024, doi: 10.1016/j.apsusc.2024.159547.

[13] J. Yang, F. Yu, A. Chen, S. Zhao, Y. Zhou, S. Zhang, T. Sun, and G. Hu, "Synthesis and application of silver and copper nanowires in high transparent solar cells," Advanced Powder Materials, vol. 1, no. 4, 2022, doi: 10.1016/j.apmate.2022.100045.

[14] M. Thirumoorthi and J. T. Prakash, "Structure, optical and electrical properties of indium tin oxide ultra-thin films prepared by jet nebulizer spray pyrolysis technique," Journal of Asian Ceramic Societies, vol. 4, no. 1, pp. 124-132, 2016, doi: 10.1016/j.jascer.2016.01.001.

[15] I. Corb, F. Manea, C. Radovan, A. Pop, G. Burtica, P. Malchev, S. Picken, and J. Schoonman, "Carbon-based composite electrodes: Preparation, characterization and application in electroanalysis," Sensors, vol. 7, pp. 2626-2635, 2007.

[16] F. Khoerunnisa, Hendrawan, Y. Sonjaya, and R. D. Hasanah, "Electrically conductive nanocomposites polymer of poly(vinyl alcohol)/glutaraldehyde/multiwalled carbon nanotubes: Preparation and characterization," Indonesian Journal of Chemistry, vol. 18, no. 3, pp. 383-389, 2018, doi: 10.22146/ijc.26620.

[17] M. Rahaman, A. Aldalbahi, L. Nayak, and R. Giri, "Electrical Conductivity of Polymer-Carbon Composites: Effects of Different Factors," pp. 159-210, 2019, doi: 10.1007/978-981-13-2688-2_5.

[18] E. Muchuweni, E. T. Mombeshora, C. M. Muiva, T. S. Sathiaraj, A. Yildiz, and D. Pugliese, "Towards high-performance dye-sensitized solar cells by utilizing reduced graphene oxide-based composites as potential alternatives to conventional electrodes: A review," Next Materials, vol. 6, 2025, doi: 10.1016/j.nxmate.2024.100477.